

Low mass Drell-Yan production of lepton pairs at forward directions at the LHC: a hybrid approach

Wolfgang Schäfer^{1,*} and Antoni Szczurek^{†1,‡}

¹*Institute of Nuclear Physics PAN, PL-31-342 Cracow, Poland*

(Dated: July 1, 2021)

Abstract

We discuss Drell-Yan production of dileptons at high energies in forward rapidity region in a hybrid high-energy approach. This approach uses unintegrated gluon distributions in one proton and collinear quark/antiquark distributions in the second proton. Corresponding momentum-space formula for the differential cross sections in high-energy approximation has been derived and will be presented. The relation to the commonly used dipole approach is discussed. We conclude and illustrate that some results of the dipole approaches are too approximate, as far as kinematics is considered, and in fact cannot be used when comparing with real experimental data. We find that the dipole formula is valid only in very forward/backward rapidity regions ($|y| > 5$) that cannot be studied experimentally in the moment. We performed calculations of some differential cross sections for low-mass dilepton production by the LHCb and ATLAS collaborations. In distinction to most of dipole approaches, we include all of the four Drell-Yan structure functions, although the impact of interference structure functions is rather small for the relevant experimental cuts. We find that both side contributions ($g + q/\bar{q}$ and $q/\bar{q} + g$) have to be included even for the LHCb rapidity coverage which is in contradiction with what is usually done in the dipole approach. We present results for different unintegrated gluon distributions from the literature (some of them include saturation effects). We see no clear hints of saturation even at small M_{ll} when comparing with the LHCb data.

PACS numbers: 13.87.-a, 11.80La, 12.38.Bx, 13.85.-t

[†] Also at University of Rzeszów, PL-35-959 Rzeszów, Poland.

*Electronic address: Wolfgang.Schafer@ifj.edu.pl

[‡]Electronic address: Antoni.Szczurek@ifj.edu.pl

I. INTRODUCTION

The Drell-Yan process of inclusive lepton-pair production is one of the important sources on the partonic structure of protons [1–3]. It was proposed some time ago that the Drell-Yan production of low invariant masses of dileptons in forward directions could be another good place in searching for the onset of (gluon) saturation [4, 5]. A number of different approaches have recently been used to calculate Drell-Yan processes in the small- x region.

In particular in recent applications for LHC much attention has been paid to the color-dipole approach [6–9], in which the main ingredient is the color dipole-nucleon cross section [10] parametrized as a function of dipole size and collision energy or a similar equivalent kinematical variable.

Alternatively a k_T -factorization approach is used to describe dilepton production. Here the recent works [11–13] are based on quark and antiquark unintegrated distributions. This formulation however is not adequate to address the nonlinear effects in the gluon distribution dubbed “saturation”. Another approach relates the small- x unintegrated quark density explicitly to the unintegrated gluon distribution [14].

Most of the above calculations, especially in the color-dipole framework do not address lepton momentum and angular distributions, but rather concentrate on a few observables, such as the dilepton invariant mass, rapidity and transverse momentum. All of these observables can be expressed through the inclusive production cross sections of a virtual heavy photon, which carries either transverse or longitudinal polarization.

For the full description of lepton distributions this is however not enough—there are interferences between transverse and longitudinal and different transverse polarization to be taken into account. The complete description of the Drell-Yan process therefore requires four structure functions [15–17].

In this paper we shall also start from the impact parameter representation, but we will perform the Fourier transformation to transverse momentum space. What then emerges [4] is a hybrid collinear/ k_T -factorization, in which the main ingredients will be collinear quark/antiquark and unintegrated gluon distributions (see e.g. [18] for predictions of forward jets in such an approach). The dominant processes captured by this approach

are shown in Fig.1. The present approach allows for explicit treatment and control of momenta of individual leptons (e^+e^- or $\mu^+\mu^-$) and therefore a comparison to existing experimental data. Below, we will also use unintegrated gluon distribution functions (UGDFs) equivalent to the dipole-nucleon cross sections known from the literature. Then a direct comparison of results from different dipole models/UGDFs with experimental data [19–21] will be possible.

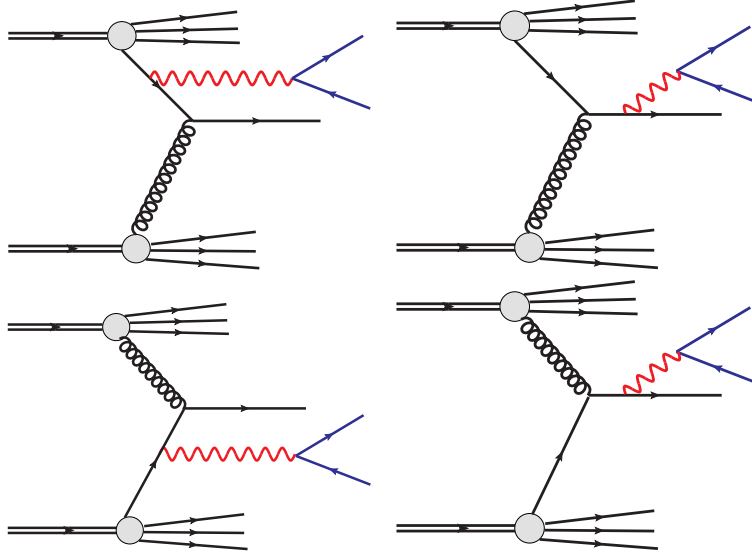


FIG. 1: The diagrams relevant for forward and backward production of dilepton pairs.

II. INCLUSIVE LEPTON PAIR PRODUCTION: KINEMATICS, FRAMES, STRUCTURE FUNCTIONS

The cross section for inclusive l^+l^- production (Drell-Yan process) can be presented as

$$(2\pi)^4 \frac{d\sigma(pp \rightarrow l^+(k_+)l^-(k_-)X)}{d^4q} = \frac{(4\pi\alpha_{\text{em}})^2}{2SM^4} \cdot W_{\mu\nu}L^{\mu\nu} \cdot d\Phi(q, k_+, k_-). \quad (1)$$

Here $q = k_+ + k_-$ is the four-momentum of the virtual photon, $q^2 = M^2$ is the invariant mass of the lepton pair. The lepton-tensor $L_{\mu\nu}$, is known explicitly:

$$L_{\mu\nu} = 4 \cdot \left(k_{+\mu}k_{-\nu} + k_{-\mu}k_{+\nu} - \frac{M^2}{2}g_{\mu\nu} \right). \quad (2)$$

All dynamical information on the production process of the virtual photon is contained in the hadronic tensor

$$W_{\mu\nu} = \int d^4x \exp(-iq \cdot x) \langle p_1 p_2 | J_\mu^{\text{em}}(0) J_\nu^{\text{em}}(x) | p_1 p_2 \rangle. \quad (3)$$

One conventionally decomposes the hadronic tensor introducing four structure functions [15, 16]:

$$W_{\mu\nu} = (\hat{x}_\mu \hat{x}_\nu + \hat{y}_\mu \hat{y}_\nu) W_T + \hat{z}_\mu \hat{z}_\nu W_L + (\hat{y}_\mu \hat{y}_\nu - \hat{x}_\mu \hat{x}_\nu) W_{\Delta\Delta} - (\hat{x}_\mu \hat{z}_\nu + \hat{z}_\mu \hat{x}_\nu) W_\Delta, \quad (4)$$

where the covariant directions $\hat{x}_\mu, \hat{y}_\mu, \hat{z}_\mu$ define the spatial axes in a rest frame of the dilepton pair (or the massive photon).

The individual structure functions can be projected out by contraction with helicity states of the massive photon as

$$\begin{aligned} W_T &= W^{\mu\nu} \epsilon_\mu^{(+)} \epsilon_\nu^{(+)*}, \quad W_L = W^{\mu\nu} \epsilon_\mu^{(0)} \epsilon_\nu^{(0)}, \\ W_\Delta &= W^{\mu\nu} (\epsilon_\mu^{(+)} \epsilon_\nu^{(0)} + \epsilon_\mu^{(0)} \epsilon_\nu^{(+)*}) \frac{1}{\sqrt{2}}, \quad W_{\Delta\Delta} = W^{\mu\nu} \epsilon_\mu^{(+)} \epsilon_\nu^{(-)*}. \end{aligned} \quad (5)$$

Here, the helicity states are defined as

$$\epsilon_\mu^{(\pm)} = -\frac{1}{\sqrt{2}} (\pm \hat{x}_\mu + i \hat{y}_\mu), \quad \epsilon_\mu^{(0)} = \hat{z}_\mu. \quad (6)$$

It is furthermore useful to introduce the time direction

$$\hat{t}_\mu = \frac{1}{M} q_\mu, \quad \hat{t}^2 = +1, \quad (7)$$

and the ‘‘spatial unit matrix’’

$$-\tilde{g}_{\mu\nu} \equiv \hat{x}_\mu \hat{x}_\nu + \hat{y}_\mu \hat{y}_\nu + \hat{z}_\mu \hat{z}_\nu = -g_{\mu\nu} + \hat{t}_\mu \hat{t}_\nu = -g_{\mu\nu} + \frac{q_\mu q_\nu}{M^2}, \quad (8)$$

To fully define the frame, we should relate the vectors $\hat{x}_\mu, \hat{y}_\mu, \hat{z}_\mu$ to the momenta of measured particles. From now on, we will use a dilepton rest-frame, in which the z -axis points along the momentum of one of the incoming protons (we choose the momentum p_2) in that frame. Such a frame is often called a Gottfried-Jackson frame. For a useful

discussion of different frame choices, see [17]. Explicitly, we have

$$\begin{aligned}
\hat{z}_\mu &= \frac{M}{q \cdot p_2} \left(p_{2\mu} - \frac{q \cdot p_2}{M^2} q_\mu \right) = \frac{M}{q \cdot p_2} \tilde{p}_{2\mu}, \\
\hat{x}_\mu &= \frac{\sqrt{-q_\perp^2}}{q \cdot p_2} \left(p_{2\mu} - \frac{q \cdot p_2}{q_\perp^2} q_{\perp\mu} \right) = \frac{M}{\sqrt{-q_\perp^2} (p_1 \cdot p_2)} \left((p_2 \cdot \hat{z}) \tilde{p}_{1\mu} - (p_1 \cdot \hat{z}) \tilde{p}_{2\mu} \right), \\
\hat{y}_\mu &= \varepsilon_{\mu\alpha\beta\gamma} \hat{x}_\alpha \hat{z}_\beta \hat{t}_\gamma = \frac{1}{\sqrt{-q_\perp^2}} \varepsilon_{\mu\alpha\beta\gamma} n_\alpha^+ n_\beta^- q_{\perp\gamma}.
\end{aligned} \tag{9}$$

Here we used the notation

$$\tilde{p}_{i\mu} \equiv \tilde{g}_{\mu\nu} p_{i\nu} = p_{i\mu} - \frac{(p_i \cdot q)}{M^2} q_\mu, \quad i = 1, 2, \tag{10}$$

as well as

$$\begin{aligned}
n_\mu^+ &= \sqrt{\frac{2}{S}} p_{1\mu}, \quad n_\mu^- = \sqrt{\frac{2}{S}} p_{2\mu}, \\
q_{\perp\mu} &= \left(g_{\mu\nu} - n_\mu^+ n_\nu^- - n_\mu^- n_\nu^+ \right) q^\nu.
\end{aligned} \tag{11}$$

Notice, that $q_{\perp\mu}$ is the transverse momentum of the virtual photon in the pp -center of mass frame. Below, boldface letters will denote the two-dimensional transverse momenta, so that e.g. $q_\perp^2 = -\mathbf{q}^2$. We will also use the notation $q_T \equiv |\mathbf{q}|$ for the absolute values of two-dimensional vectors.

Now, performing explicitly the contraction of leptonic and hadronic tensor expressed in the chosen basis, we obtain the inclusive dilepton cross section as

$$\begin{aligned}
\frac{d\sigma(pp \rightarrow l^+ l^- X)}{dx_+ dx_- d^2\mathbf{k}_+ d^2\mathbf{k}_-} &= \frac{\alpha_{\text{em}}}{(2\pi)^2 M^2} \frac{x_F}{x_+ x_-} \left\{ \Sigma_T(x_F, \mathbf{q}, M^2) D_T\left(\frac{x_+}{x_F}\right) + \Sigma_L(x_F, \mathbf{q}, M^2) D_L\left(\frac{x_+}{x_F}\right) \right. \\
&\quad + \Sigma_\Delta(x_F, \mathbf{q}, M^2) D_\Delta\left(\frac{x_+}{x_F}\right) \left(\frac{\mathbf{l}}{|\mathbf{l}|} \cdot \frac{\mathbf{q}}{|\mathbf{q}|} \right) \\
&\quad \left. + \Sigma_{\Delta\Delta}(x_F, \mathbf{q}, M^2) D_{\Delta\Delta}\left(\frac{x_+}{x_F}\right) \left(2 \left(\frac{\mathbf{l}}{|\mathbf{l}|} \cdot \frac{\mathbf{q}}{|\mathbf{q}|} \right)^2 - 1 \right) \right\}.
\end{aligned} \tag{12}$$

We use the light-cone parametrization of particle momenta:

$$\begin{aligned}
k_\mu^\pm &= x_\pm \sqrt{\frac{S}{2}} n_\mu^\pm + \frac{\mathbf{k}_\pm^2}{x_\pm \sqrt{2S}} n_\mu^\mp + k_{\perp\mu}^\pm, \\
q_\mu &= x_F \sqrt{\frac{S}{2}} n_\mu^+ + \frac{M^2 + \mathbf{q}^2}{x_F \sqrt{2S}} n_\mu^- + q_{\perp\mu}.
\end{aligned} \tag{13}$$

so that

$$x_F = x_+ + x_-, \mathbf{q} = \mathbf{k}_+ + \mathbf{k}_-. \quad (14)$$

We also need the light-cone relative transverse momentum

$$\mathbf{l} = \frac{x_+}{x_F} \mathbf{k}_- - \frac{x_-}{x_F} \mathbf{k}_+. \quad (15)$$

The functions $D_i, i \in \{T, L, \Delta, \Delta\Delta\}$ come from the contractions of the leptonic tensor and describe the $\gamma^* \rightarrow l^+ l^-$ transition. They are given by

$$\begin{aligned} D_T(u) &= 4(u^2 + (1-u)^2), \\ D_L(u) &= D_{\Delta\Delta}(u) = 8u(1-u), \\ D_{\Delta}(u) &= 4\sqrt{u(1-u)}(2u-1). \end{aligned} \quad (16)$$

Finally, the functions $\Sigma_i(x_F, \mathbf{q}, M^2), i \in \{T, L, \Delta, \Delta\Delta\}$ parametrize the density matrix of production of the massive photon. Expressed in terms of helicity eigenstates, we have for the density matrix

$$\rho_{\lambda\lambda'} \frac{d\sigma(pp \rightarrow \gamma^*(M^2)X)}{dx_F d^2\mathbf{q}} = \frac{1}{x_F} \frac{\alpha_{\text{em}}}{8\pi^2 S} W_{\mu\nu} \epsilon_\mu^{(\lambda)} \epsilon_\nu^{(\lambda')*}. \quad (17)$$

Or

$$\rho_{\lambda\lambda'} = \frac{W_{\mu\nu} \epsilon_\mu^{(\lambda)} \epsilon_\nu^{(\lambda')*}}{2W_T + W_L}, \rho_{++} + \rho_{--} + \rho_{00} = 1. \quad (18)$$

Above we used the components

$$\Sigma_i(x_F, \mathbf{q}, M^2) = \rho_i \frac{d\sigma(pp \rightarrow \gamma^*(M^2)X)}{dx_F d^2\mathbf{q}} \equiv \frac{1}{x_F} \frac{\alpha_{\text{em}}}{8\pi^2 S} W_i, \quad i \in T, L, \Delta, \Delta\Delta. \quad (19)$$

III. THE PARTON LEVEL PROCESS: $qp \rightarrow \gamma^* X$

Let us now turn to the parton-level description of the Drell-Yan process. What we ultimately need are the hadron-level density matrix elements for the $pp \rightarrow \gamma^* X$ process. As we are interested in the ‘‘forward region’’ of phase space, it is reasonable to assume that the most important degrees of freedom will be quarks and antiquarks from one of the protons and small- x gluons from the second one. Our parton level subprocess will

therefore look like an excitation of the γ^*q -Fock state of an incoming quark in the small- x gluon field of the second hadron.

We follow the notation and normalization of [22], and can write down the density-matrix for production of the virtual photon in the $qp \rightarrow \gamma^*X$ process as

$$\hat{\rho}_{\lambda\lambda'} \frac{d\hat{\sigma}(qp \rightarrow \gamma^*(z, \mathbf{q})X)}{dzd^2\mathbf{q}} = \frac{1}{2(2\pi)^2} \overline{\sum}_{\sigma, \sigma'} \int d^2\mathbf{r}d^2\mathbf{r}' \exp[-i\mathbf{q}(\mathbf{r} - \mathbf{r}')] \psi_{\sigma\sigma'}^{(\lambda)}(z, \mathbf{r}) \psi_{\sigma\sigma'}^{(\lambda')*}(z, \mathbf{r}') \times (\sigma(x_2, z\mathbf{r}) + \sigma(x_2, z\mathbf{r}') - \sigma(x_2, z(\mathbf{r} - \mathbf{r}'))). \quad (20)$$

The light-front wave functions for the $q_\sigma \rightarrow \gamma_\lambda^*q'_\sigma$ transition (here σ, σ', λ denote the helicities of particles) read:

$$\begin{aligned} \psi_{\sigma\sigma'}^{(\lambda)}(z, \mathbf{r}) &= \int \frac{d^2\mathbf{q}}{(2\pi)^2} \exp[-i\mathbf{r}\mathbf{q}] \psi_{\sigma\sigma'}^{(\lambda)}(z, \mathbf{q}) \\ &= e_q \sqrt{z(1-z)} \int \frac{d^2\mathbf{q}}{(2\pi)^2} \exp[-i\mathbf{r}\mathbf{q}] \frac{\bar{u}_{\sigma'}(1-z, -\mathbf{q}) \epsilon_\mu^{(\lambda)*} \gamma_\mu u_\sigma(1, \mathbf{0})}{\mathbf{q}^2 + \varepsilon^2}, \end{aligned} \quad (21)$$

with $\varepsilon^2 = (1-z)M^2 + z^2m_q^2$.

To derive the momentum-space k_T -factorization representation, we use the relation of the dipole cross section with the unintegrated gluon distribution

$$\sigma(x, \mathbf{r}) = \frac{1}{2} \int d^2\boldsymbol{\kappa} f(x, \boldsymbol{\kappa}) (1 - \exp[i\boldsymbol{\kappa}\mathbf{r}]) (1 - \exp[-i\boldsymbol{\kappa}\mathbf{r}]). \quad (22)$$

Where $f(x, \boldsymbol{\kappa})$ is

$$f(x, \boldsymbol{\kappa}) = \frac{4\pi\alpha_S}{N_c} \frac{1}{\boldsymbol{\kappa}^4} \frac{\partial G(x, \boldsymbol{\kappa}^2)}{\partial \log \boldsymbol{\kappa}^2}. \quad (23)$$

Inserting (21) and (22) into Eq. (20), we obtain:

$$\begin{aligned} \hat{\rho}_{\lambda\lambda'} \frac{d\hat{\sigma}(qp \rightarrow \gamma^*(z, \mathbf{q})X)}{dzd^2\mathbf{q}} &= \frac{1}{2(2\pi)^2} \overline{\sum}_{\sigma, \sigma'} \int d^2\boldsymbol{\kappa} f(x_2, \boldsymbol{\kappa}) \\ &(\psi_{\sigma\sigma'}^{(\lambda)}(z, \mathbf{q}) - \psi_{\sigma\sigma'}^{(\lambda)}(z, \mathbf{q} - z\boldsymbol{\kappa})) (\psi_{\sigma\sigma'}^{(\lambda')*}(z, \mathbf{q}) - \psi_{\sigma\sigma'}^{(\lambda')*}(z, \mathbf{q} - z\boldsymbol{\kappa}))^* \end{aligned} \quad (24)$$

From here, we obtain the impact-factor representation for the elements of the density matrix of production $\hat{\Sigma}_i$, where $i = T, L, \Delta, \Delta\Delta$,

$$\hat{\Sigma}_i(z, \mathbf{q}, M^2) = \hat{\rho}_i \frac{d\hat{\sigma}(qp \rightarrow \gamma^*(z, \mathbf{q})X)}{dzd^2\mathbf{q}} = \frac{e_q^2 \alpha_{\text{em}}}{2N_c} \int \frac{d^2\boldsymbol{\kappa}}{\pi\boldsymbol{\kappa}^4} \alpha_S(\bar{q}^2) \mathcal{F}(x_2, \boldsymbol{\kappa}^2) I_i(z, \mathbf{q}, \boldsymbol{\kappa}), \quad (25)$$

with

$$\begin{aligned}
I_T(z, \mathbf{q}, \boldsymbol{\kappa}) &= \frac{1 + (1 - z)^2}{z} |\boldsymbol{\Phi}|^2 + z^3 m_q^2 \Phi_0^2, \\
I_L(z, \mathbf{q}, \boldsymbol{\kappa}) &= \frac{4(1 - z)^2 M^2}{z} \Phi_0^2, \\
I_\Delta(z, \mathbf{q}, \boldsymbol{\kappa}) &= \frac{2(2 - z)(1 - z)M}{z} \left(\frac{\mathbf{q}}{|\mathbf{q}|} \cdot \boldsymbol{\Phi} \right) \Phi_0, \\
I_{\Delta\Delta}(z, \mathbf{q}, \boldsymbol{\kappa}) &= \frac{2(1 - z)}{z} \left(|\boldsymbol{\Phi}|^2 - 2 \left(\frac{\mathbf{q}}{|\mathbf{q}|} \cdot \boldsymbol{\Phi} \right)^2 \right), \tag{26}
\end{aligned}$$

where

$$\begin{aligned}
\boldsymbol{\Phi}(z, \mathbf{q}, \boldsymbol{\kappa}) &= \frac{\mathbf{q}}{\mathbf{q}^2 + \varepsilon^2} - \frac{\mathbf{q} - z\boldsymbol{\kappa}}{(\mathbf{q} - z\boldsymbol{\kappa})^2 + \varepsilon^2}, \\
\Phi_0(z, \mathbf{q}, \boldsymbol{\kappa}) &= \frac{1}{\mathbf{q}^2 + \varepsilon^2} - \frac{1}{(\mathbf{q} - z\boldsymbol{\kappa})^2 + \varepsilon^2}. \tag{27}
\end{aligned}$$

A brief comment on our k_T -factorization form of the Drell-Yan cross section is in order. An important property of Eq.(25) is its linear dependence of the unintegrated glue. This linear dependence remains valid even in the presence of multiple scattering effects which become important in the presence of a large saturation scale. In fact all possible saturation effects get absorbed into the nonlinear evolution [23, 24] of the unintegrated gluon distribution.

The origin of this simplification is the fact, that the emitted photon does not couple to the exchanged gluon [25]. Indeed for the analogous $q \rightarrow qg$ transition relevant to the production of forward jets, the linear k_T -factorization is strongly violated, and the relevant saturation effects are not exhausted by the nonlinear evolution of the unintegrated glue [26].

In a language, where interactions of the fast quark with the target is described by the correlators of Wilson lines, see e.g. [27], the above simplification manifests itself through the fact that the cross section depends only on the correlator of two fundamental Wilson lines. Higher order correlation functions, which would have their own evolution equations [28], do not appear.

Therefore there is a sound theoretical motivation behind the search for saturation effects on the unintegrated glue by means of the forward Drell-Yan process.

IV. k_T -FACTORIZATION FORM OF THE DILEPTON CROSS SECTION AT THE HADRON LEVEL

To go to the hadron level, we will assume the collinear factorization on the quark side and write, choosing a factorization scale $\mu^2 \sim \mathbf{q}^2 + \varepsilon^2$:

$$\begin{aligned} \Sigma_i(x_F, \mathbf{q}, M) &= \sum_f \int dx_1 dz \delta(x_F - zx_1) \left[q_f(x_1, \mu^2) + \bar{q}_f(x_1, \mu^2) \right] \hat{\Sigma}_i(z, \mathbf{q}, M^2). \\ &= \sum_f \frac{e_f^2 \alpha_{\text{em}}}{2N_c} \int_{x_F}^1 dx_1 \left[q_f(x_1, \mu^2) + \bar{q}_f(x_1, \mu^2) \right] \int \frac{d^2 \boldsymbol{\kappa}_2}{\pi \boldsymbol{\kappa}_2^4} \mathcal{F}(x_2, \boldsymbol{\kappa}_2) \alpha_S(\bar{q}^2) I_i\left(\frac{x_F}{x_1}, \mathbf{q}, \boldsymbol{\kappa}_2\right). \end{aligned} \quad (28)$$

The full dilepton cross section is then

$$\begin{aligned} \frac{d\sigma(pp \rightarrow l^+ l^- X)}{dy_+ dy_- d^2 \mathbf{k}_+ d^2 \mathbf{k}_-} &= x_+ x_- \frac{d\sigma(pp \rightarrow l^+ l^- X)}{dx_+ dx_- d^2 \mathbf{k}_+ d^2 \mathbf{k}_-} \\ &= \frac{\alpha_{\text{em}}^2}{8\pi^2 N_c M^2} \sum_f e_f^2 \int_{x_F}^1 dx_1 \left[x_1 q_f(x_1, \mu^2) + x_1 \bar{q}_f(x_1, \mu^2) \right] \int \frac{d^2 \boldsymbol{\kappa}_2}{\pi \boldsymbol{\kappa}_2^4} \mathcal{F}(x_2, \boldsymbol{\kappa}_2) \alpha_S(\bar{q}^2) \\ &\quad \left\{ \frac{x_F}{x_1} I_T\left(\frac{x_F}{x_1}, \mathbf{q}, \boldsymbol{\kappa}_2\right) D_T\left(\frac{x_+}{x_F}\right) + \frac{x_F}{x_1} I_L\left(\frac{x_F}{x_1}, \mathbf{q}, \boldsymbol{\kappa}_2\right) D_L\left(\frac{x_+}{x_F}\right) \right. \\ &\quad + \frac{x_F}{x_1} I_\Delta\left(\frac{x_F}{x_1}, \mathbf{q}, \boldsymbol{\kappa}_2\right) D_\Delta\left(\frac{x_+}{x_F}\right) \left(\frac{\mathbf{l}}{|\mathbf{l}|} \cdot \frac{\mathbf{q}}{|\mathbf{q}|}\right) \\ &\quad \left. + \frac{x_F}{x_1} I_{\Delta\Delta}\left(\frac{x_F}{x_1}, \mathbf{q}, \boldsymbol{\kappa}_2\right) D_{\Delta\Delta}\left(\frac{x_+}{x_F}\right) \left(2\left(\frac{\mathbf{l}}{|\mathbf{l}|} \cdot \frac{\mathbf{q}}{|\mathbf{q}|}\right)^2 - 1\right) \right\}. \end{aligned} \quad (29)$$

If we also want to include the recoiling jet, we can do this by inserting the delta-functions

$$dx_J \delta(x_J + x_F - x_1) d^2 \mathbf{k}_J \delta^{(2)}(\boldsymbol{\kappa}_2 - \mathbf{q} - \mathbf{k}_J). \quad (30)$$

This gives us the fully differential spectrum

$$\begin{aligned} \frac{d\sigma(pp \rightarrow l^+ l^- X)}{dy_+ dy_- dy_J d^2 \mathbf{k}_+ d^2 \mathbf{k}_- d^2 \mathbf{k}_J} &= \frac{\alpha_{\text{em}}^2}{8\pi^3 N_c M^2} \frac{x_F x_J}{x_F + x_J} \\ &\quad \times \sum_f e_f^2 \left[q_f(x_F + x_J, \mu^2) + \bar{q}_f(x_F + x_J, \mu^2) \right] \frac{\alpha_S(\bar{q}^2) \mathcal{F}(x_2, \mathbf{q} + \mathbf{k}_J)}{(\mathbf{q} + \mathbf{k}_J)^4} \\ &\quad \times \left\{ I_T^f\left(\frac{x_F}{x_F + x_J}, \mathbf{q}, \mathbf{q} + \mathbf{k}_J\right) D_T\left(\frac{x_+}{x_F}\right) \right. \\ &\quad + I_L^f\left(\frac{x_F}{x_F + x_J}, \mathbf{q}, \mathbf{q} + \mathbf{k}_J\right) D_L\left(\frac{x_+}{x_F}\right) \\ &\quad \left. + I_\Delta^f\left(\frac{x_F}{x_F + x_J}, \mathbf{q}, \mathbf{q} + \mathbf{k}_J\right) D_\Delta\left(\frac{x_+}{x_F}\right) \left(\frac{\mathbf{l}}{|\mathbf{l}|} \cdot \frac{\mathbf{q}}{|\mathbf{q}|}\right) \right\} \end{aligned}$$

$$+ I_{\Delta\Delta}^f\left(\frac{x_F}{x_F + x_J}, \mathbf{q}, \mathbf{q} + \mathbf{k}_J\right) D_{\Delta\Delta}\left(\frac{x_+}{x_F}\right) \left[2\left(\frac{\mathbf{l}}{|\mathbf{l}|} \cdot \frac{\mathbf{q}}{|\mathbf{q}|}\right)^2 - 1\right] \}. \quad (31)$$

Rapidities are obtained as:

$$y_i = \log\left(\frac{x_i \sqrt{S}}{\sqrt{\mathbf{k}_i^2}}\right) \leftrightarrow x_i = \sqrt{\frac{\mathbf{k}_i^2}{S}} \cdot e^{y_i}, \quad i = +, -, J. \quad (32)$$

The longitudinal momentum fractions x_1, x_2 entering the quark and gluon distributions are then

$$\begin{aligned} x_1 &= x_F + x_J = x_+ + x_- + x_J = \sqrt{\frac{\mathbf{k}_+^2}{S}} e^{y_+} + \sqrt{\frac{\mathbf{k}_-^2}{S}} e^{y_-} + \sqrt{\frac{\mathbf{k}_J^2}{S}} e^{y_J}, \\ x_2 &= \sqrt{\frac{\mathbf{k}_+^2}{S}} e^{-y_+} + \sqrt{\frac{\mathbf{k}_-^2}{S}} e^{-y_-} + \sqrt{\frac{\mathbf{k}_J^2}{S}} e^{-y_J}. \end{aligned} \quad (33)$$

For completeness the invariant mass of the dilepton system is

$$M^2 = m_{\perp+}^2 + m_{\perp-}^2 + 2m_{\perp+}m_{\perp-} \cosh(y_+ - y_-) - \mathbf{q}^2, \quad m_{\perp\pm} = \sqrt{\mathbf{k}_{\pm}^2 + m_{\pm}^2}. \quad (34)$$

V. FIRST RESULTS

In the present paper we shall use different UGDFs known from the literature. The Kimber-Martin-Ryskin distributions [29] make a simple link to collinear distributions. In this approach the transverse momentum distribution of “initial” gluons originates from the last emission in the ladder. In the present calculations we use MSTW08 distributions [30] to generate the KMR unintegrated gluon distributions. Here we use numerical implementation by Maciula and Szczurek used e.g. in the production of charm and double charm [31]. For the forward emissions considered here rather low longitudinal momentum fractions enter into the calculations. In this region a nonlinear effects and onset of saturation may be, at least potentially, important. The nonlinear effects were implemented e.g. in Ref.[32]. These distributions give a nice description of forward exclusive production of J/ψ mesons [33]. In addition, for reference, we shall use also a simple Golec-Biernat and Wüsthoff (GBW) parametrization [34] and unintegrated gluon distribution obtained from a dipole-nucleon cross section solving the Balitsky-Kovchegov equation [23, 24], published in [35] which we will name in the present paper AASM UGDF for brevity. See the appendix for a description of the numerical procedure.

For the quark and antiquark distributions we use MSTW08 leading-order distributions [30]. For most of the calculations we used $M_{\tilde{l}}^2$ both as a factorization and renormalization scales. We have also tried:

$$\begin{aligned}\mu_R^2 &= \max\left(\kappa_{\perp}^2, q_{\perp}^2 + \varepsilon^2\right), \\ \mu_F^2 &= q_{\perp}^2 + \varepsilon^2.\end{aligned}\tag{35}$$

The corresponding results turned out to be almost identical.

A. Full rapidity range

Before going to predictions for particular experiments we wish to discuss the general situation for the whole phase space, i.e. in the broad range of lepton rapidities.

In Fig.2 we show a two-dimensional distribution in rapidities of positively and negatively charged leptons. One can observe that the contribution of the $(q/\bar{q})g \rightarrow l^+l^-(q/\bar{q})$ process extends into a quite broad range, also into the region of negative rapidities of positively (y_+) and negatively (y_-) charged leptons. Similar contribution of the $g(q/\bar{q}) \rightarrow l^+l^-j$ subprocess would be trivially symmetric around the $(y_+ = 0, y_- = 0)$ point. The calculation was done with the leading-order MSTW08 quark/antiquark distributions and the Kimber-Martin-Ryskin UGDF [29]. The figure clearly shows that including only one of the contributions is not sufficient but we wish to stress that this is routinely done in the dipole approach (see e.g.[7, 8]).

The rapidities of both leptons are strongly correlated i.e. $y_+ \approx y_-$. Distribution in rapidity of the dileptons may be particularly interesting. In Fig.3 we show such distributions for different UGDFs from the literature. Quite different results are obtained for different UGDFs. It is obvious that at the rapidity of the lepton pair $y_* \approx 0$ both side mechanisms (gq/\bar{q} or $q/\bar{q}g$) must be included. At $y_* = 0$ they give exactly the same contribution. This is not correctly treated in the dipole approaches where only one side contribution is included.

In contrast to leading-order collinear approach, in our approach dileptons have finite transverse momenta. In Fig.4 we show two-dimensional distributions in rapidity and transverse momentum of dileptons. One can see that at large (positive) rapidities the

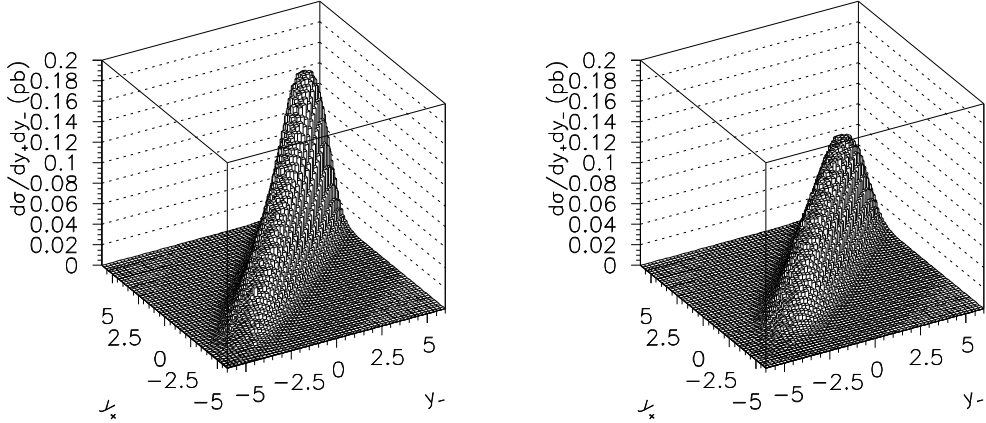


FIG. 2: Two-dimensional (y_+, y_-) distribution for $\sqrt{s} = 7$ TeV and $k_{T+}, k_{T-} > 3$ GeV for MSTW08 PDF and KMR (left) and KS (right) UGDFs.

span of transverse momenta is significantly broader. This effect was not discussed so far in the literature. In our case the effect is inherently related to the models of UGDFs used in the calculation. Practically all models of UGDFs predict such an effect. It would be interesting to observe/verify such an effect experimentally at the LHC.

In the traditional dipole approach the produced jet (quark or antiquark) is not taken into account explicitly into the kinematics of the process. In our calculations it enters in the calculation of parton momentum fractions: x_1 (gluon distribution) and x_2 (quark/antiquark distribution). In Fig.5 we demonstrate the effect when the part of x_i corresponding to the jet emission (see Eq.(33)) is neglected. The largest effect is obtained when y_* is large i.e. when both charged leptons are produced very forward. This is also the region when saturation, or more generally nonlinear effects, are expected. Therefore one should be very careful in interpreting agreement or disagreement of any calculation in this region. We shall return to the problem in the context of LHCb kinematics.

In the calculations performed so far both valence and sea quark/antiquark collinear distributions are included. Fig.6 demonstrates the role of valence quark distributions (compare the solid (all components) and the dashed (valence quarks only) lines). The contribution related to valence quark distributions is concentrated at $y_* > 0$. Only

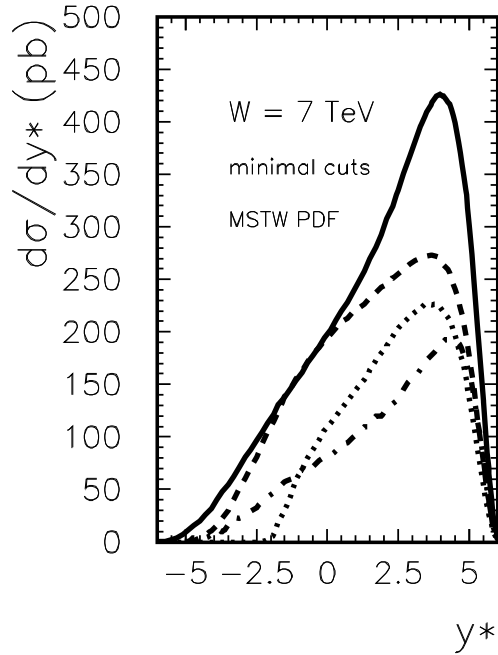


FIG. 3: Distribution in rapidity of the dileptons for $\sqrt{s} = 7$ TeV and $k_{T+}, k_{T-} > 3$ GeV for MSTW08 PDF and different UGDFs: KMR (solid), KS (dashed), AAMS (dotted) and GBW (dash-dotted).

the sea quark/antiquark contribution extends to the region of $y_* < 0$. This region is neglected in the most dipole model approaches in the literature. The LHCb region is dominated by the valence component. We do not need to mention in this context that the valence quark distributions are well known and therefore in this region of rapidities one can test models of UGDFs, provided kinematics of the process is correctly taken into account as discussed already above.

B. LHCb

In this subsection we show results relevant for the LHCb collaboration results [19]. The LHCb configuration, due to its specificity ($2.0 < \eta < 4.5$), allows to test very asymmetric longitudinal momentum fractions of partons. This is potentially interesting

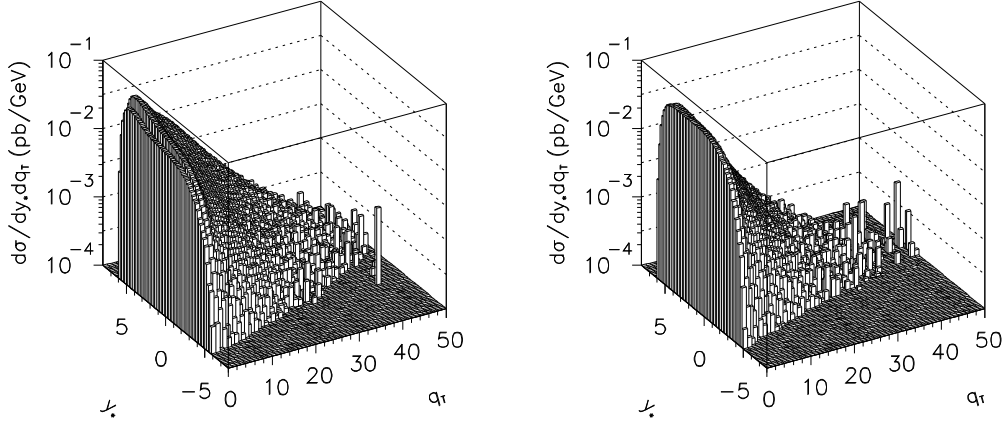


FIG. 4: Two-dimensional (y_*, q_T) distribution for $\sqrt{s} = 7$ TeV and $k_{T+}, k_{T-} > 3$ GeV for MSTW08 PDF and KMR (left) and KS (right) UGDF.

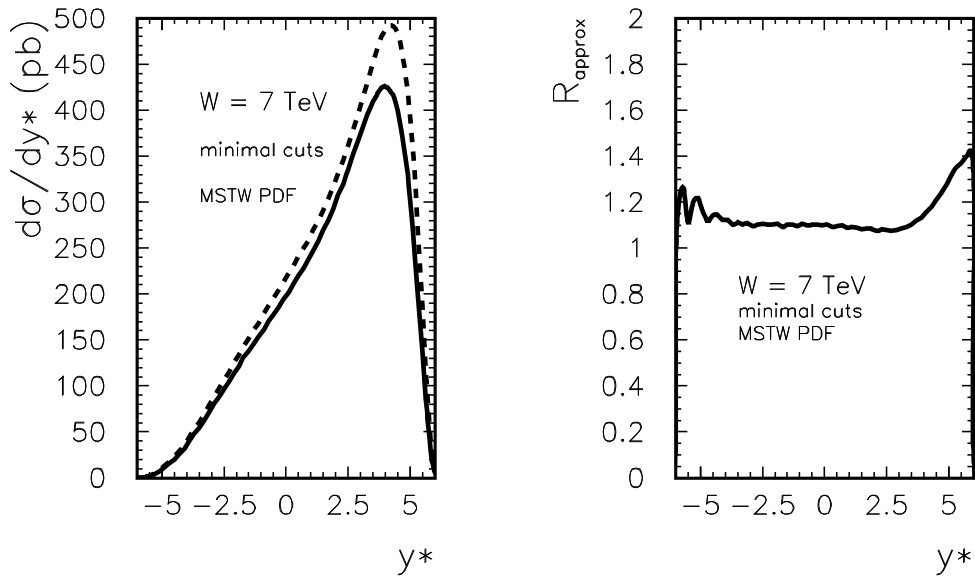


FIG. 5: Distribution in y_* for exact (solid) and approximate (dashed) formula for calculating x_1 and x_2 for $\sqrt{s} = 7$ TeV and $k_{T+}, k_{T-} > 3$ GeV for MSTW08 PDF and KMR UGDF. In the right panel we show the ratio of the two distributions.

in the context of searches for onset of nonlinear effects and/or saturation which are

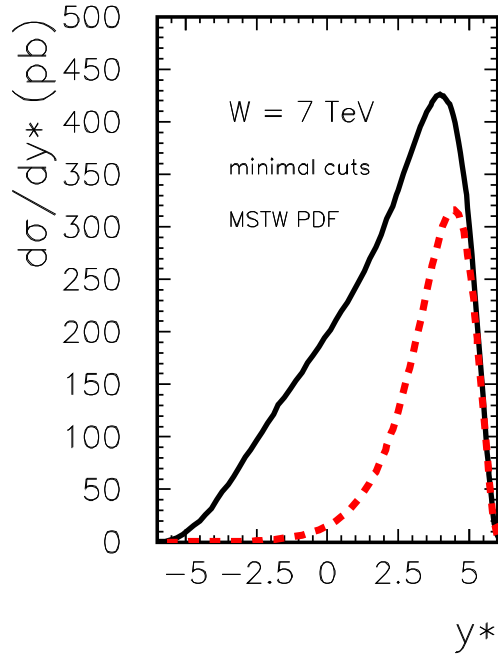


FIG. 6: Distribution in rapidity of the dileptons for $\sqrt{s} = 7$ TeV and $k_{T+}, k_{T-} > 3$ GeV for MSTW08 valence quark distributions and KMR UGDFs.

expected to occur in the region of very small- x of gluons.

Dilepton invariant mass distribution is traditionally the most popular observable in the context of Drell-Yan processes. In Fig.7 we show invariant mass distribution for different UGDFs from the literature.

In naive leading-order collinear calculation charged leptons are produced back-to-back. In the k_T -factorization approach presented here this is dramatically different. In Fig.8 we discuss correlations in lepton transverse momenta. For the KMR UGDF the transverse momenta are much less correlated than e.g. for the KS or AAMS UGDFs. In the latter cases they are enhanced for $k_{T+} = k_{T-}$.

The same effect can be demonstrated in one-dimensional distribution in transverse momentum of the dilepton pairs. Very different distributions are obtained for different UGDFs. It would be interesting to compare the results of our calculations with experimental data.

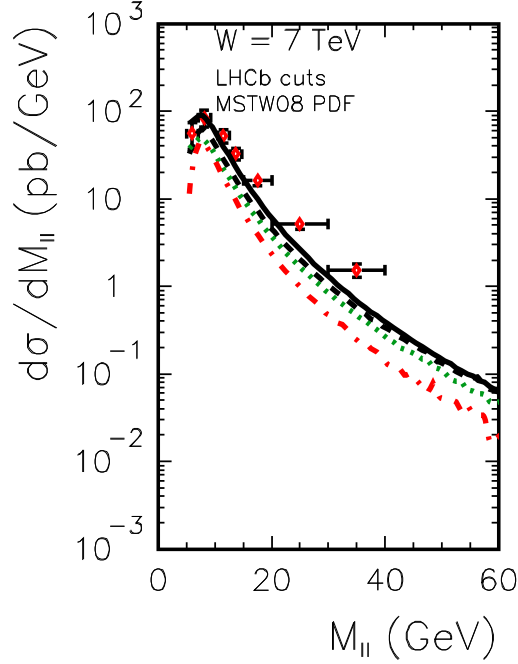


FIG. 7: Invariant mass distribution (only the dominant component) for the LHCb cuts: $2 < y_+, y_- < 4.5, k_{T+}, k_{T-} > 3$ GeV for different UGDFs: KMR (solid), Kutak-Stasto (dashed), AAMS (dotted) and GBW (dash-dotted).

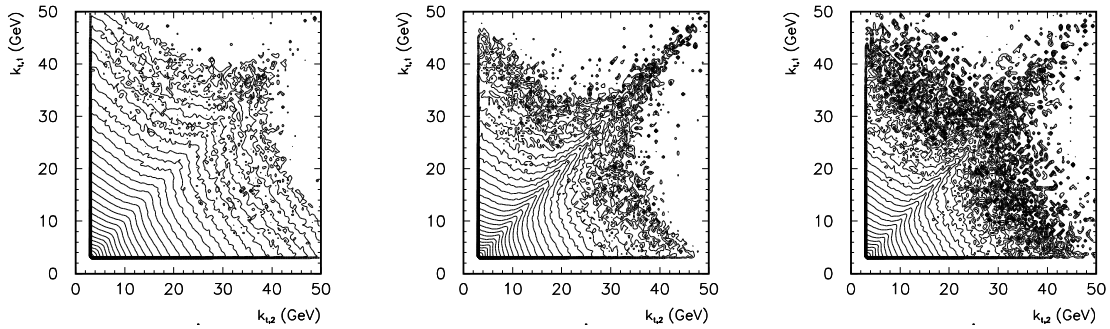


FIG. 8: Two-dimensional (k_{T+}, k_{T-}) distribution for $\sqrt{s} = 7$ TeV and $k_{T+}, k_{T-} > 3$ GeV for MSTW08 PDF and KMR (left), KS (middle) and AAMS (right) UGDFs.

In Fig.10 we show the invariant mass distribution as well as the T and L contributions separately. We see that the T contribution is significantly larger than the L contribution,

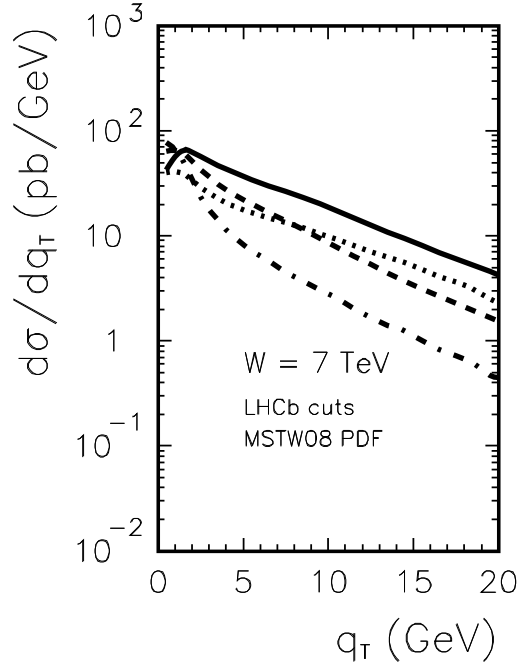


FIG. 9: Dilepton transverse momentum distribution (only the dominant component) for the LHCb cuts: $2 < y_+, y_- < 4.5$, $k_{T+}, k_{T-} > 3$ GeV for different UGDFs: KMR (solid), Kutak-Stasto (dashed), AAMS (dotted) and GBW (dash-dotted).

especially for large dilepton invariant masses.

Now we wish to illustrate the role of the interference terms. Let us define the quantity:

$$R_{int} = \frac{d\sigma_{all} - d\sigma_{T+L}}{d\sigma_{all}}. \quad (36)$$

As an example in Fig.11 we show the so-defined quantity as a function of dilepton invariant mass for the LHCb kinematics. One can observe very small effect of including interference terms of the order of 1 %. The fluctuations of the theoretical curve are due to the Monte Carlo method and smallness of the effect.

So far we have considered only $g + q/\bar{q}$ contribution. Now we wish to discuss how important is the second-side (subdominant) $q/\bar{q} + g$ contribution for the LHCb kinematics. In Fig.12 we show both the dominant (dashed) and subdominant (dotted) contributions as well as their sum (solid). Clearly the subdominant contribution is not negligible.

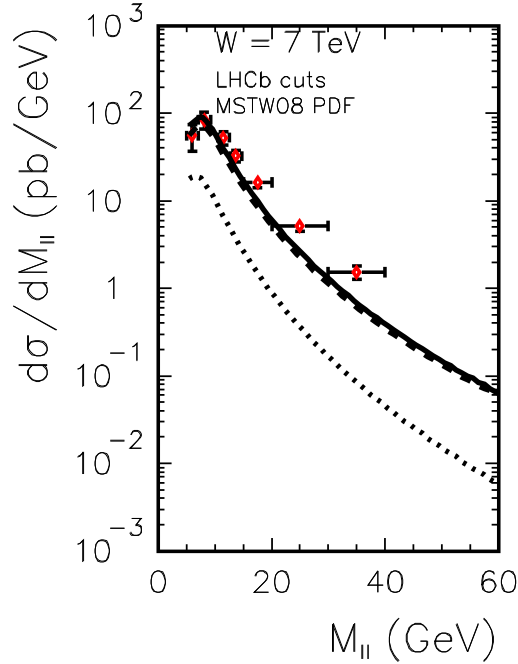


FIG. 10: The T and L contributions to the dilepton invariant mass distribution for the LHCb kinematics: $2 < y_+, y_- < 4.5$, $k_{T+}, k_{T-} > 3$ GeV. KMR UGDF was used here.

C. ATLAS

In this subsection we show similar results for the low- M_{ll} ATLAS data [21]. The ATLAS detector covers more central rapidity range ($-2.4 < y_+, y_- < 2.4$) and imposes a slightly larger lower cut on the dilepton transverse momenta $k_{T+}, k_{T-} > 6$ GeV.

The invariant mass distribution for the ATLAS kinematics is shown in Fig.13. We get relatively good agreement with the ATLAS data for dilepton invariant masses M_{ll} at the threshold. At larger dilepton invariant mass some strength is clearly missing. Here longitudinal momentum fractions are typically $x_1, x_2 \sim 0.01-0.1$. This is a region where antiquark distributions are dominated by the meson cloud effects (see e.g. [36]). Some effects of the type of $q\bar{q}$ annihilation are clearly not included in the present approach (as well as in the dipole approach), at least for the considered range of x_1, x_2 .

The transverse momenta of leptons are correlated as shown in Fig. 14. We observe a

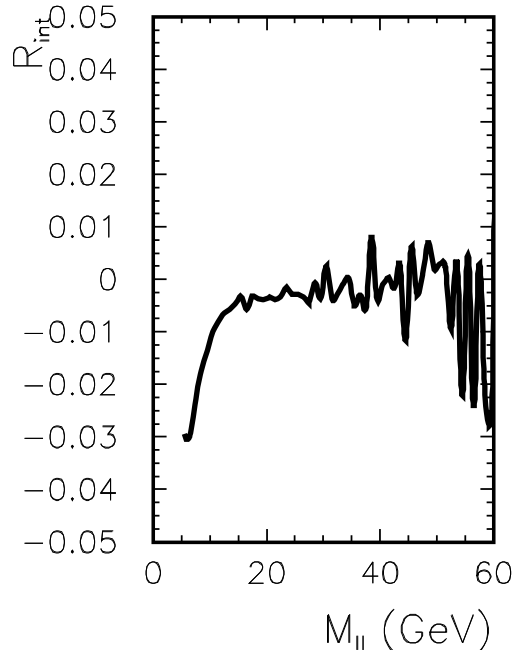


FIG. 11: The R_{int} as a function of M_{ll} for the LHCb kinematics: $2 < y_+, y_- < 4.5$, $k_{T+}, k_{T-} > 3$ GeV. KMR UGDF was used here. The fluctuations are due to insufficient statistics of our Monte Carlo calculation.

clear ridge along $k_{T+} = k_{T-}$ and enhancements when either k_{T+} or k_{T-} are small.

Distributions in transverse momentum of the dilepton pairs are shown in Fig.15 for the different UGDFs. This plot reminds corresponding plot for the LHCb kinematics.

VI. SUMMARY AND CONCLUSIONS

In the present paper we have considered Drell-Yan production of dileptons in the forward rapidity region in a hybrid high-energy approach. In this approach the main ingredients are collinear quark/antiquark distributions and unintegrated gluon distributions. Corresponding formula for matrix element in high-energy approximation has been derived and presented. The relation to the commonly used dipole approach has been discussed. In contrast to the dipole approach our formulation correctly treats the kinematic of the process and can be applied to the analysis of real experimental data

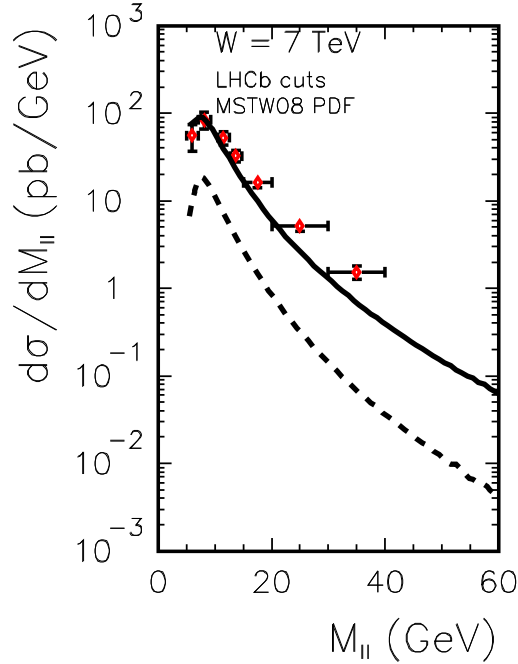


FIG. 12: Contributions of the second-side component for the LHCb kinematics: $2 < y_+, y_- < 4.5$, $k_{T+}, k_{T-} > 3$ GeV. KMR UGDF was used here.

including their specific kinematic cuts. In our more general formula we have obtained four terms instead of two (T, L) in the standard dipole model.

A corresponding program including underlying $2 \rightarrow 3$ subprocess matrix elements ($g + q/\bar{q} \rightarrow l^+l^-j$ or $q/\bar{q} + g \rightarrow l^+l^-j$), PDFs and UGDFs has been constructed. To illustrate our approach we have performed calculations of differential cross sections corresponding to recent experimental results for low-mass dilepton production by the LHCb and ATLAS collaborations. In the first calculation we have used different UGDFs from the literature and MSTW08 quark/antiquark distributions. Relatively good agreement with the experimental data has been achieved for small M_{ll} . Some strength at larger M_{ll} is missing which is probably due to lack of meson cloud effects, not included here.

In contrast what was done in the literature, we have found that both side contributions have to be included even for the LHCb configuration. For the ATLAS kinematics this gives half of the cross section.

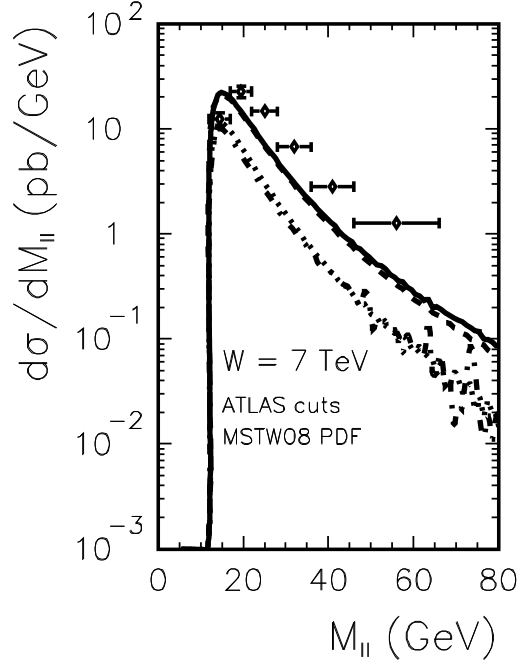


FIG. 13: Invariant dilepton mass distribution for the ATLAS kinematics: $-2.4 < y_+, y_- < 2.4$, $k_{T+}, k_{T-} > 6$ GeV. Here both gq/\bar{q} and $q/\bar{q}g$ contributions have been included.

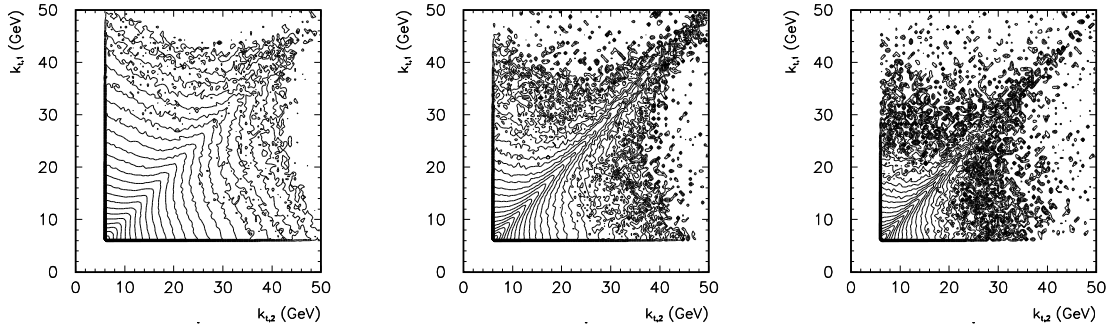


FIG. 14: Lepton transverse momentum correlations for the ATLAS kinematics: $-2.4 < y_+, y_- < 2.4$, $k_{T+}, k_{T-} > 6$ GeV. The left panel is for the KMR UGDF, the middle panel for the KS UGDF and the right panel for the AAMS UGDF.

We have found that the contribution of individual terms ($i = T, L, \dots$) strongly depends on kinematical variables (such as M_{ll}) as well as on cuts. We have quantified

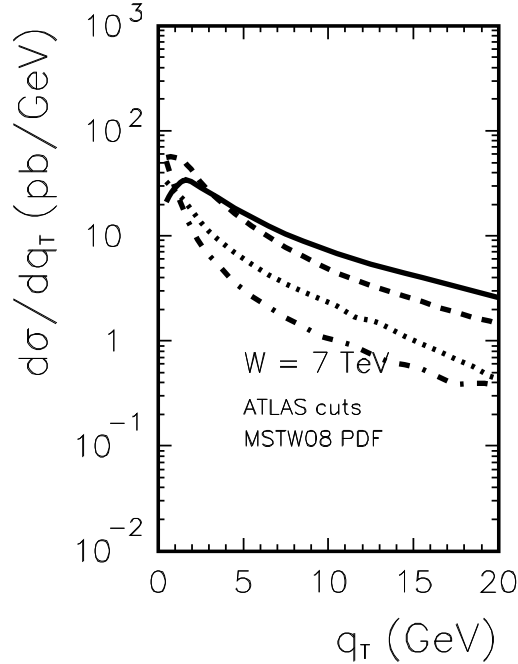


FIG. 15: Transverse momentum distribution of dileptons for the ATLAS kinematics: $-2.4 < y_+, y_- < 2.4, k_{T+}, k_{T-} > 6$ GeV for MSTW08 PDF and for different UGDFs: KMR (solid), KS (dashed), AAMS (dotted) and GBW (dash-dotted).

the effect of the new interference terms not present explicitly in the dipole approach. We have found that the missing strength at larger M_{ll} could be due to e.g. meson cloud effects and the perturbative gluon component alone considered here may be not sufficient.

We do not see clear hints of saturation at small M_{ll} . We wish to stress also that this region of the phase space is potentially difficult for extracting the Drell-Yan contribution due to potential contamination of double semi-leptonic decays of charmed and/or bottom mesons or baryons which is slightly model (Monte Carlo) dependent.

Acknowledgments

We are indebted to Rafal Maciula for help in adopting our program to a Monte Carlo form. This study was partially supported by the Polish National Science Centre grant DEC-2014/15/B/ST2/02528.

Appendix A: Unintegrated gluon distribution from dipole cross sections

The dipole cross section is related to the unintegrated glue as

$$\sigma(x, \mathbf{r}) = \frac{4\pi}{N_c} \int \frac{d^2\boldsymbol{\kappa}}{\boldsymbol{\kappa}^4} \alpha_S \mathcal{F}(x, \boldsymbol{\kappa}) \{1 - \exp(i\boldsymbol{\kappa}\mathbf{r})\}. \quad (\text{A1})$$

The parametrizations of [35] are presented in the form

$$\sigma(x, \mathbf{r}) = \sigma_0 \cdot N(x, \mathbf{r}), \quad (\text{A2})$$

with $N(x, \mathbf{r}) \rightarrow 1$ at large \mathbf{r} . We can therefore easily obtain, that

$$\frac{\alpha_S \mathcal{F}(x, \boldsymbol{\kappa})}{\boldsymbol{\kappa}^4} = \frac{\sigma_0 N_c}{4\pi} \int \frac{d^2\mathbf{r}}{(2\pi)^2} \exp(-i\boldsymbol{\kappa}\mathbf{r}) [1 - N(x, \mathbf{r})], \quad (\text{A3})$$

or

$$\mathcal{F}(x, \boldsymbol{\kappa}) = \frac{\sigma_0 N_c}{8\pi^2} \frac{\boldsymbol{\kappa}^2}{\alpha_S(\boldsymbol{\kappa}^2)} \int_0^\infty r dr J_0(\kappa r) [1 - N(x, \mathbf{r})], \quad (\text{A4})$$

where $J_0(x)$ is the Bessel function. The Fourier-Bessel (or Hankel-) transform (A4) can pose severe numerical problems, if values at large $\boldsymbol{\kappa}^2$ are required. For the evaluations of these integrals we use therefore a dedicated code FFTLog [37] which is based on the algorithm of [38].

-
- [1] S. D. Drell and T. M. Yan, Phys. Rev. Lett. **25**, 316 (1970) [Phys. Rev. Lett. **25**, 902 (1970)].
 - [2] R. K. Ellis, W. J. Stirling and B. R. Webber, “QCD and collider physics,” Camb. Monogr. Part. Phys. Nucl. Phys. Cosmol. **8** (1996) 1.
 - [3] J. C. Peng and J. W. Qiu, Prog. Part. Nucl. Phys. **76**, 43 (2014) [arXiv:1401.0934 [hep-ph]].

- [4] F. Gelis and J. Jalilian-Marian, Phys. Rev. D **66**, 094014 (2002) [hep-ph/0208141].
- [5] F. Gelis and J. Jalilian-Marian, Phys. Rev. D **76**, 074015 (2007) [hep-ph/0609066].
- [6] M. B. G. Ducati, M. T. Griep and M. V. T. Machado, Phys. Rev. D **89**, no. 3, 034022 (2014) [arXiv:1307.6882 [hep-ph]].
- [7] K. Golec-Biernat, E. Lewandowska and A. M. Stasto, Phys. Rev. D **82**, 094010 (2010) [arXiv:1008.2652 [hep-ph]].
- [8] E. Basso, V. P. Goncalves, J. Nemchik, R. Pasechnik and M. Sumbera, Phys. Rev. D **93**, 034023 (2016) doi:10.1103/PhysRevD.93.034023 [arXiv:1510.00650 [hep-ph]].
- [9] L. Motyka, M. Sadzikowski and T. Stebel, JHEP **1505**, 087 (2015) [arXiv:1412.4675 [hep-ph]].
- [10] N. N. Nikolaev and B. G. Zakharov, Z. Phys. C **49**, 607 (1991).
- [11] A. Szczurek and G. Slipek, Phys. Rev. D **78** (2008) 114007 [arXiv:0808.1360 [hep-ph]].
- [12] M. A. Nefedov, N. N. Nikolaev and V. A. Saleev, Phys. Rev. D **87** (2013) 1, 014022 [arXiv:1211.5539 [hep-ph]].
- [13] S. P. Baranov, A. V. Lipatov and N. P. Zotov, Phys. Rev. D **89** (2014) 9, 094025 [arXiv:1402.5496 [hep-ph]].
- [14] F. Hautmann, M. Hentschinski and H. Jung, Nucl. Phys. B **865**, 54 (2012) [arXiv:1205.1759 [hep-ph]].
- [15] R.J. Oakes, Nuovo Cimento A **44**, 440 (1966).
- [16] C. S. Lam and W. K. Tung, Phys. Rev. D **18**, 2447 (1978).
- [17] D. Boer and W. Vogelsang, Phys. Rev. D **74**, 014004 (2006) [hep-ph/0604177].
- [18] M. Deak, F. Hautmann, H. Jung and K. Kutak, JHEP **0909**, 121 (2009) [arXiv:0908.0538 [hep-ph]].
- [19] [The LHCb collaboration], “Inclusive low mass Drell-Yan production in the forward region at $\sqrt{s}=7$ TeV ,” LHCb-CONF-2012-013; Conference report prepared for XX International Workshop on Deep-Inelastic Scattering and Related Subjects, 26-30, March 2012, Bonn, Germany.
- [20] S. Chatrchyan *et al.* [CMS Collaboration], JHEP **1312**, 030 (2013) [arXiv:1310.7291 [hep-ex]].

- [21] G. Aad *et al.* [ATLAS Collaboration], JHEP **1406**, 112 (2014) [arXiv:1404.1212 [hep-ex]].
- [22] N. N. Nikolaev and W. Schäfer, Phys. Rev. D **71**, 014023 (2005) [hep-ph/0411365].
- [23] I. Balitsky, Nucl. Phys. B **463**, 99 (1996) [hep-ph/9509348].
- [24] Y. V. Kovchegov, Phys. Rev. D **60**, 034008 (1999) [hep-ph/9901281].
- [25] N. N. Nikolaev, W. Schäfer and B. G. Zakharov, Phys. Rev. Lett. **95**, 221803 (2005) [hep-ph/0502018].
- [26] N. N. Nikolaev, W. Schäfer, B. G. Zakharov and V. R. Zoller, Phys. Rev. D **72**, 034033 (2005) [hep-ph/0504057].
- [27] F. Dominguez, C. Marquet, B. W. Xiao and F. Yuan, Phys. Rev. D **83**, 105005 (2011) [arXiv:1101.0715 [hep-ph]].
- [28] E. Iancu and D. N. Triantafyllopoulos, JHEP **1111**, 105 (2011) [arXiv:1109.0302 [hep-ph]].
- [29] M. A. Kimber, A. D. Martin, and M. G. Ryskin, Eur. Phys. J. C **12**, 655 (2000) [hep-ph/9911379]; Phys. Rev. D **63**, 114027 (2001) [hep-ph/0101348].
- [30] A. D. Martin, W. J. Stirling, R. S. Thorne and G. Watt, Eur. Phys. J. C **63**, 189 (2009) [arXiv:0901.0002 [hep-ph]].
- [31] R. Maciula and A. Szczurek, Phys. Rev. **D87** (2013) 094022; A. van Hameren, R. Maciula and A. Szczurek, Phys. Rev. **D89** (2014) 094019; R. Maciula, A. Szczurek and M. Luszczak, Phys. Rev. **D92** (2015) 054006.
- [32] K. Kutak and A. M. Stasto, Eur. Phys. J. C **41**, 343 (2005) [hep-ph/0408117].
- [33] A. Cisek, W. Schäfer and A. Szczurek, JHEP **1504**, 159 (2015) [arXiv:1405.2253 [hep-ph]].
- [34] K. J. Golec-Biernat and M. Wüsthoff, Phys. Rev. D **59**, 014017 (1998) [hep-ph/9807513].
- [35] J. L. Albacete, N. Armesto, J. G. Milhano and C. A. Salgado, Phys. Rev. D **80**, 034031 (2009) [arXiv:0902.1112 [hep-ph]].
- [36] H. Holtmann, A. Szczurek and J. Speth, Nucl. Phys. A **596**, 631 (1996) [hep-ph/9601388]; N. N. Nikolaev, W. Schäfer, A. Szczurek and J. Speth, Phys. Rev. D **60**, 014004 (1999) [hep-ph/9812266].
- [37] A. J. S. Hamilton, Mon. Not. Roy. Astron. Soc. **312**, 257 (2000) [astro-ph/9905191]; <http://casa.colorado.edu/~ajsh/FFTLlog/>
- [38] J. D. Talman, J. Comp. Phys. **29**, 35 (1978).